Title: Clam-like cyclotricatechylene-based capsules: identifying the roles of protonation state and guests as well as the drivers for stability and (anti-)cooperativity

Authors: Nisha Mehta, BSc, MSc; Brendan F. Abrahams, BSc, PhD; Lars Goerigk, Diplomchemiker, PhD

To be cited as: Chem. Asian J. 10.1002/asia.201901767

Link to VoR: https://doi.org/10.1002/asia.201901767

Clam-like cyclotricatechylene-based capsules: identifying the roles of protonation state and guests as well as the drivers for stability and (anti-)cooperativity

Nisha Mehta, Brendan F. Abrahams, and Lars Goerigk*

School of Chemistry, The University of Melbourne, Parkville, Victoria 3010, Australia

E-mail: lars.goerigk@unimelb.edu.au

Abstract

Cyclotricatechylene ($ctcH_6$) is a bowl-shaped macrocyclic compound that can be used as a building block for self-assembled capsules. $ctcH_6$ and its derivatives in various protonation states—here collectively labeled as CTC—form dimers that resemble the shape of a clam. These clam-shaped entities have been studied experimentally by Abrahams, Robson, and co-workers [B. F. Abrahams, N. J. FitzGerald, T. A. Hudson, R. Robson and T. Waters, *Angew. Chem. Int. Ed.* **2009**, *48*, 3129-3132] where the capsules acted as an excellent host for large alkali metal cations. In this study, we present a detailed analysis based on accurate dispersion-corrected Density Functional Theory approaches that reveals the factors that stabilise such CTC-based capsules at different protonation states and their interaction with various encapsulated guests. Our results show that the capsules' overall stability results as an interplay of hydrogen bonding, London dispersion, and electrostatic effects. The most stable capsules with group-1 and group-2 cations as guests contain only six phenolic hydrogens, as opposed

to the maximum possible number of twelve. Inclusion of larger alkali metal cations is favoured due to larger London-dispersion contributions. Cations are favoured as guests over isoelectronic neutral species, as the resulting host-guest complexes experience additional stability due to cooperative effects. In fact, using the latter to drive the formation of specific capsules could be used in future strategies aimed at synthesising similar aggregates; our results provide an insightful understanding and useful guidance for such future endeavours.

1 Introduction

Molecular capsules are supramolecules that are often used in host-guest chemistry for various potential applications, such as sensing of molecules and ions,[1] stabilising short-lived molecular species,[2,3] and using the capsules as nano reaction vessels.[4–8] The interactions between guest and host can be covalent[9] or ionic in nature,[10] explained through hydrogen-bonding effects,[7,8,11–13] metal-ligand coordination,[14–18] or hydrophobic interactions,[19] or a combination of all the aforementioned effects.[20,21]

One of the many examples for a host molecule that non-covalently captures its guest is the macrocyclic compound cyclotriveratrylene (CTV), which assumes a bowl-shaped crown conformation.[22] As such, CTV is analogous to the well-known calix[n]arenes that have a range of applications in supramolecular chemistry.[23–25] The applications of CTV and its derivatives include their usage as ligands in host-guest chemistry,[26–29] in sensors, in soft materials, or in separations of fullerene mixtures.[22,30,31]

Cyclotricatechylene ($ctcH_6$) (Figs 1a and b) is a demethylated form of CTV. Its phenolic hydrogens can be used to form hydrogen-bonded aggregates. In this work, we focus on the hydrogen-bonded dimers of cyclotricatechylene and its various deprotonated forms, with the latter being collectively abbreviated with "CTC" in the following. Such CTC-based dimers assume a shape that resemble that of a clam (Fig. 1c).[33] A particularly interesting feature of this clam-type aggregate is its tendency to enclose various cations that mostly

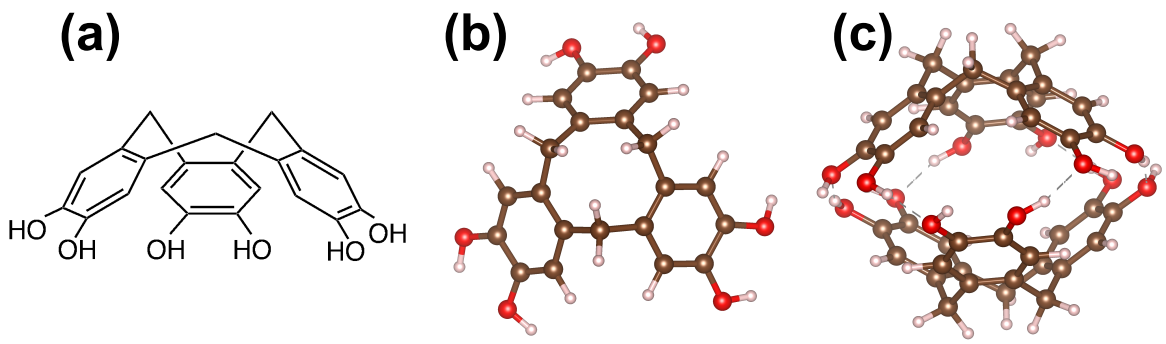

Figure 1: Structure of cyclotricatechylene ($ctcH_6$) **(a,b)** and a clam-like cyclotricatechylene dimer $(ctcH_6)_2$ **(c)**. The structures in parts b) and c) were optimised at the PBEh-3c[32] level of theory.

interact with the aromatic systems of the CTC units.[33] Various combinations of CTC ligands with appropriate cations, such as alkali-metal cations, have been characterised in recent years by Abrahams, Robson and co-workers.[33–35] In this context we note that the isolation of alkali metal cations—especially from aqueous solution—is particularly challenging due to large entropies of solution,[36] but CTC-based capsules offer a promising route towards achieving this task. The previous works identified stable clam-like units with the composition $[Rb(ctcH_5)(ctcH_4)]^{2-}$ in the crystal structure of $[C(NH_2)_3]_2[Rb(ctcH_5)(ctcH_4)]\cdot 15H_2O$.[33] The two separate bowl-shaped CTC units are held together by six hydrogen bonds, with average phenolic oxygen-oxygen distances of 2.46 - 2.69 Å. The Rb^+ ion interacts with the six aromatic rings of both CTC halves. The clam adopts a closed arrangement. The $Rb_2[Rb(ctcH_5)(ctcH_4)]\cdot 3.5\ H_2O$ crystal also possesses a very similar $[Rb(ctcH_5)(ctcH_4)]^{2-}$ clam-like structure. Closely related clam-like units were found in the $[C(NH_2)_3]_2[Cs(ctcH_5(ctcH_4)]\cdot 2(CH_3)_2CO\cdot 5H_2O$ crystal structure. The above findings showed the tendency of CTC-based clams for Cs^+ and Rb^+. A quite remarkable feature is their tendency to associate with the aromatic π systems instead of enclosed water or the phenolic groups, which are present in abundance. In the same study, attempts to form a capsule that enclosed K^+ were unsuccessful. Instead, the ion associated with aromatic π surfaces of a single $ctcH_5$ unit.

The experimental results for CTC-based clams are limited to alkali-metal cations i.e. Rb^+,

Cs^+ and K^+, as well as NMe_4^+ and NEt_4^+. In the case of NMe_4^+ and NEt_4^+, the clams partially open up in order to accommodate a large cation.[33] Although CTC-based anionic dimers showed a tendency for large alkali metal cations, there are still open questions. The aforementioned studies were limited to a few selective protonation states; i.e. $[Rb(ctcH_5)(ctcH_4)]^{2-}$, $[Cs(ctcH_5)(ctcH_4)]^{2-}$, $[Rb(ctcH_5)_2]^-$ and $[Cs(ctcH_5)_2]^-$. These clam-like units were identified in crystal structures with different counterions, e.g. $[Rb(ctcH_5)(ctcH_4)]^{2-}$ units were identified in $[C(NH_2)_3]_2[Rb(ctcH_5)(ctcH_4)]\cdot 15H_2O$ and $Rb_2[Rb(ctcH_5)(ctcH_4)]\cdot 3.5H_2O$, $[Cs(ctcH_5)(ctcH_4)]^{2-}$ in $[C(NH_2)_3]_2[Cs(ctcH_5)(ctcH_4)]\cdot 2(CH_3)_2CO\cdot 5H_2O$, while a single $K(ctcH_5)^-$ unit was identified in $K(ctcH_5)\cdot C_2H_5OH$. However, to better understand the formation of such capsules, it is important to treat all systems on an equal footing. Herein, we aim to carry out such a treatment and would like to facilitate our understanding of the main structural motif for different protonation states. In particular, we intend to illuminate the driving force of the clam's stability, what system-specific characteristics support the binding strength between the two CTC monomers, and how the nature of the guest influences the overall stability. Moreover, these clam-like units have never been explored with small alkali metal cations, group-2 dications, or noble-gas atoms, with the latter being isoelectronic to the group-1 and group-2 cations. Their investigation gives rise to structurally diverse systems, which we will address herein.

The most efficient way to tackle our open questions is via computational chemistry. In fact, some of our questions can only be answered with computational means. Advances in Density Functional Theory (DFT) methods have reached a point that allows reliably predicting properties with very good to high accuracy—for a recent account on the 'zoo' of DFT methods and how to determine reliable DFT-based strategies for applications, see Ref. 37— and we will use such state-of-the-art methods to provide answers to the aforementioned open questions to guide future syntheses of these and related compounds.

We start our discussion with an overview of our computational strategy and then proceed with a detailed evaluation of Cs^+ based clams. These insights are then compared to CTC-

based systems with other guests (i.e. Rb^+, K^+, Na^+, Li^+, Ba^{2+}, Sr^{2+}, Ca^{2+}, Mg^{2+}, Be^{2+}, Xe, Kr, Ar, Ne and He). We conclude with a discussion of our results and recommendations that will provide an insightful understanding, useful guidance and potential direction of future syntheses of these and similar systems.

2 Outline of the computational strategy

2.1 Determination of the most stable isomers

The starting point of this study is the determination of the most stable protonation states for each species. Doing such an analysis with DFT methods would be very resource-demanding due to a large number of possible isomers in each protonation state, with the exception to the fully protonated and deprotonated capsules. Instead, we opted for a time-efficient sampling based on Grimme's semi-empirical GFN2-xTB molecular orbital (MO) theory, which has been designed to work well for geometries, vibrational frequencies, and noncovalent interactions.[38] It and its predecessor GFN-xTB[39] have also been suggested as a first step in the screening for conformers, isomers, and protonation sites.[38,40,41] While it is now available in different quantum chemistry codes, we used GFN2-xTB with Grimme's standalone program.[42]

Our protocol to sample through the various protonation states shall be exemplified here for the $(CTC)_2$-Cs^+ system. The initial coordinates were extracted from the experimental $[Cs(ctcH_6)_2Cl]$ crystal structure.[43] Thus, this structure has a total of 12 phenolic hydrogens (see Fig. 1); herein we refer to this system as being in "protonation state 12". In order to obtain other protonation states, we gradually removed protons from the phenolic groups, and just explored additional systems ranging from protonation state 11 to protonation state 0—the completely deprotonated capsule. For partially protonated states (protonation state 11 to 1), we also generated all possible isomers. In total, we automatically generated 4096 of such structures that were used for an initial sampling via single-point calculations at

the GFN2-xTB level. Note that from an efficiency perspective, we did not screen for any potential duplicates at this stage, as such a process would have taken longer than running calculations with GFN2-xTB for all structures. For each protonation state, we determined the lowest energy isomer and used it as a baseline to determine the relative energies with respect to the other isomers. Isomers that fell outside a 2 kcal/mol energy window with respect to the lowest-energy isomer were discarded.

The remaining structures were then optimised at the B97-3c level of theory.[44] The resulting lowest-energy B97-3c structure for each protonation state was then further optimised at the PBEh-3c[32] hybrid-DFT level. Both levels of theory are low-cost DFT methods that provide a proper description of London-dispersion effects[45,46] and reasonably accurate geometries and properties taking into account corrections for truncated atomic-orbital basis sets; for more details see the original literature.[32,44] The final structures are provided in the Supporting Information (SI). A similar protocol was used for systems with other guests. Whenever an experimental structure was not available, we used the most stable Cs^+-based one as an input and simply replaced the cation.

The DFT-based geometry optimisations were performed using Turbomole 7.3,[47–49] with Turbomole's multigrid option "m4" for the numerical integration of the exchange-correlation potentials.[50] The self-consistent-field (SCF) calculations were carried out with a convergence criterion of $10^{-7}E_h$. The geometry convergence criterion with respect to the change in total energy between two optimisation cycles was set to 10^{-7} E_h. As the previous experiments were performed in solution, one should take into account the effects of solvents, as they may change in the structural features and relative stabilities of the systems. In addition, we did not include counterions for efficiency reasons, which resulted in some of the considered systems to be highly negatively charged. To avoid the resulting well-known problem of unbound electrons in many DFT approaches, it is therefore a standard "tool" to avoid such unphysical states through screening negative charges via a solvent model, which additionally improves SCF convergence.[51–53] Therefore, we employed the conductor-like screening model

(COSMO)[54] with water as the solvent to be consistent with the experiments. All COSMO calculations employed Turbomole's default settings and a dielectric constant of ϵ=80.4. In this context, note that GFN2-xTB's own implicit solvent model for water was applied during the protonation-state screening to ensure consistency with the remainder our study.[39]

All calculations involving the heavier elements, i.e. Cs, Rb, Xe, Ba, Sr, made use of effective core potentials of the def2-ecp type to better describe core-electronic effects.[55]

2.2 Detailed analysis of noncovalent interactions

Single point energy calculations were carried out on the PBEh-3c optimised structures to further analyse energetic properties. For that purpose we employed the ωB97M-V functional,[56] which includes a van-der-Waals-DFT type dispersion correction.[57] It was shown to be the most accurate and robust hybrid functional and a good alternative to double-hybrid functionals for large systems in recently performed benchmark studies that were the largest of their kind.[37,58–61] Like other van-der-Waals DFT methods, only two-body contributions to the dispersion energy are included. As we are also interested in analysing potential non-additive three-body effects, we followed the example by Risthaus and Grimme[62] and enhanced the van-der-Waals-DFT type dispersion correction with the three-body term known from Grimme's DFT-D3 correction.[45] In accordance with Ref. 62, we use the suffix "+E^{ABC}" in combination with our chosen level of theory to highlight this type of enhancement; for a more detailed discussion of the shortcomings of van-der-Waals DFT methods for many-body effects, see Ref. 63. Note that our study is the first to suggest to use a three-body term in conjunction with the ωB97M-V functional. ORCA4.1.2 and ORCA4.2.0 were employed for ωB97M-V,[64] while Grimme's standalone program DFTD3[65] was used to obtain the DFT-D3 type three-body correction based on the DFT-D3 parametrisation of ωB97M-V recently introduced by Najibi and Goerigk.[58]

Solvent effects in ORCA were simulated with the conductor-like polarisable continuum model (CPCM) and the same dielectric constant for water as before. We used Ahlrichs-type triple-

ζ basis set def2-TZVP[55] for all ωB97M-V calculations with an SCF convergence criterion of $10^{-7}\mathrm{E}_h$, and a multigrid procedure with ORCA's numerical quadrature grid '3' until SCF convergence and a final post-SCF step with grid '4'. We used the van-der-Waals-DFT dispersion correction in the post-SCF version, as implemented in ORCA, as this approach can speed up the overall calculation by a factor of 2 for large systems without compromising the underlying method's accuracy.[58]

An important characteristic to analyse in supramolecular chemistry is the (relative) strength of noncovalent interactions, as this analysis can provide valuable insights into what drives the formation of such assemblies and how to better control them. In our case, we can see the host-guest complexes as trimers, with the individual monomers being the guest ion/atom and the two CTC units, which may both be protonated equally or differently, being the hosts. Herein, we analyse interaction energies without taking geometry-relaxation effects into account, as is common in such studies.[62,66–70] In other words, when calculating interaction energies, the monomers assume the same internal coordinates as in the bound trimer. As such, the total interaction energy ΔE can be calculated as:

$$\Delta E = E_{123} - E_1 - E_2 - E_3, \tag{1}$$

where E_{123} is the total energy of the trimer and $E_{1/2/3}$ the total energies of the individual monomers. While our main focus is on the actual interaction energies, we tested the effect of geometry relaxation for one example, namely a single CTC unit in $[\mathrm{Cs(ctcH_3)_2}]^{5-}$. The deformation energy to go from the free CTC unit to the distorted unit in the capsule is 14.5 kcal/mol at the ωB97M-V/def2-TZVP+E^{ABC} level of theory.

A more detailed analysis of the interaction energy of a trimer can be achieved by expressing its interaction energy as:

$$\Delta E = \Delta E_{12} + \Delta E_{23} + \Delta E_{13} + \Delta E_3, \tag{2}$$

where the terms ΔE_{ij} (with $i, j = 1, 2, 3$) are dimer interaction energies of the three possible dimers that can be formed, namely the two CTC units without the guest, or the guest with either of the two CTC units. The dimer interaction energies, are therefore defined as:

$$\Delta E_{ij} = E_{ij} - E_i - E_j \tag{3}$$

The term ΔE_3 in Eq. 2 is a three-body intermolecular interaction term that is calculated through total energies of the trimer, the three possible dimers and the three monomers:[71,72]

$$\Delta E_3 = E_{123} - E_{12} - E_{23} - E_{13} + E_1 + E_2 + E_3 \tag{4}$$

The term that describes this three-body intermolecular interaction is particularly insightful, as it allows the analysis of cooperativity in the formation of the capsules. The trivial case is ΔE_3=0, which means that the trimer interaction energy is merely the sum of the three individual dimer interaction energies. If, however, ΔE_3<0, we observe that the three-body intermolecular interaction term induces additional stability due to cooperative effects. Alternatively, if ΔE_3>0, we can talk about anti-cooperative effects.

In addition to the quantitative analysis described above, we will also occasionally present a qualitative visualisation of the different components to the resulting interaction energy through NCIPLOTs.[73,74] If carried out on a converged wavefunction (or density), plots are possible that show areas that are governed by dispersion forces, hydrogen bonds, and repulsive interactions. As the individual components can currently not be separately plotted for our system due to limitations of the program, we only report such plots in the SI (Figs S3 - S4). More instructive plots are based on attractive intermolecular interactions (hydrogen bonds and dispersion forces); this option is only implemented for promolecular densities. Such plots turned out to be more insightful and are reported in the main manuscript.

In order to grasp the interactions between the clams and the guest, we occasionally present plots of the molecular electrostatic potential (MESP). MESPs were generated at the PBEh-3c

level using Turbomole 7.3.

3 Results and discussion

3.1 Clams with Cs^+ as the guest

3.1.1 Structural characteristics

As outlined in the introduction, CTC-based clams have a tendency to use their phenolic hydrogens to form hydrogen-bonded dimers that result in a clam-like assembly. A particularly interesting feature of this clam is its tendency to enclose guests. This section considers a large alkali metal cation, namely Cs^+, as the guest. The previous experimental study of Cs^+ based clam-like structures was limited to the $[Cs(ctcH_5)(ctcH_4)]^{2-}$ and $[Cs(ctcH_5)_2]^-$ systems (protonation states 9 and 10, respectively);[33] therefore, it is important to explore the structure and stabilities of this system at all possible protonation states of the CTC units' phenolic hydrogens. In Section 2.1, we outlined how we generated all possible isomers and obtained the lowest-energy structures for each protonation state. In the $[Cs(ctcH_6)_2]^+$ structure (Fig. 2a), the two shell-like CTC components are bound together by six symmetric hydrogen bonds of the type H−O···H−O each with a length of 1.78 Å. Cs^+ is located at the centre of the clam. All six oxygens at the rim of a single CTC unit are nearly co-planar. The twelve aromatic carbons bound to the methylene groups make closest contact with the Cs^+ centre (shortest Cs^+-C distance, 3.51 Å).

In $[Cs(ctcH_6)(ctcH_5)]$, $[Cs(ctcH_5)_2]^-$, $[Cs(ctcH_5)(ctcH_4)]^{2-}$, $[Cs(ctcH_4)_2]^{3-}$, $[Cs(ctcH_4)(ctcH_3)]^{4-}$, some H−O···H−O bonds are replaced by hydrogen bonds of the type O^-···H−O, namely in one case for $[Cs(ctcH_6)(ctcH_5)]$ with a gradual increase of one O^-···H−O bond for the series until six bonds of that type have been established for $[Cs(ctcH_3)_2]^{5-}$ (protonation state 6). As such hydrogen bonds are shorter than the ones of the type H−O···H−O (see Fig. 3), some of the resulting structures are asymmetric and can be described as slightly "opened up"

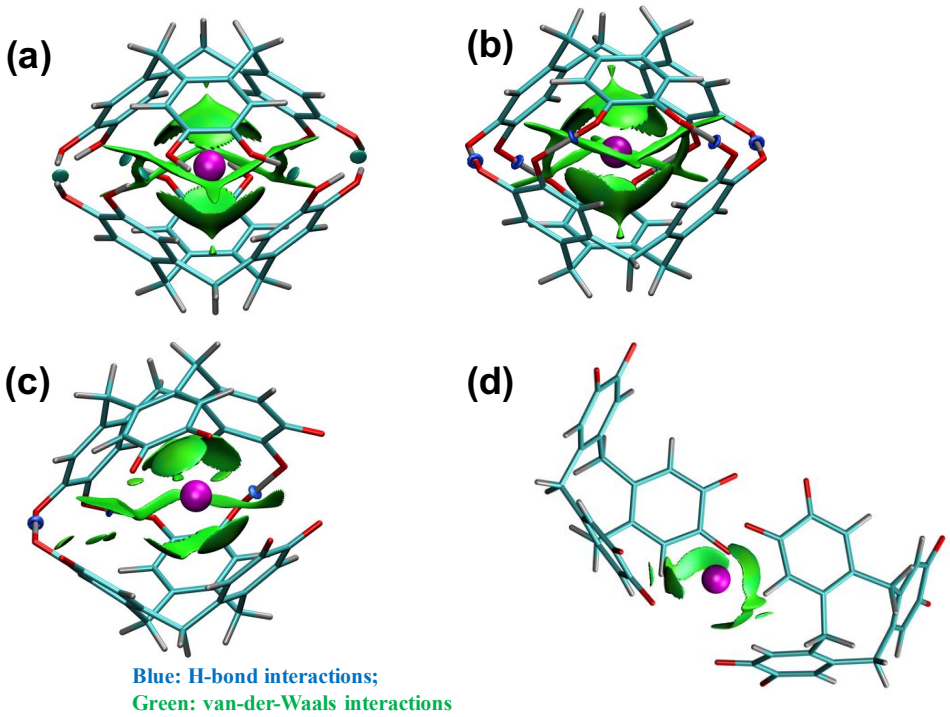

Figure 2: PBEh-3c optimised structures and their NCIPLOT isosurfaces of $[Cs(ctcH_6)_2]^+$ **(a)**, $[Cs(ctcH_3)_2]^{5-}$ **(b)**, $[Cs(ctcH_2)(ctcH)]^{2-}$ **(c)** and $[Cs(ctc)_2]^{11-}$ **(d)**. The isosurfaces were generated for a density value of 0.09 a.u. and a reduced density gradient value of 0.3 a.u. The plots show the intermolecular non-covalent interactions between three interacting units. Van-der-Waals interaction regions and hydrogen bond interactions are highlighted in the insets. All hydrogens are shown in silver, oxygens in red, carbons in cyan, and caesium in ochre.

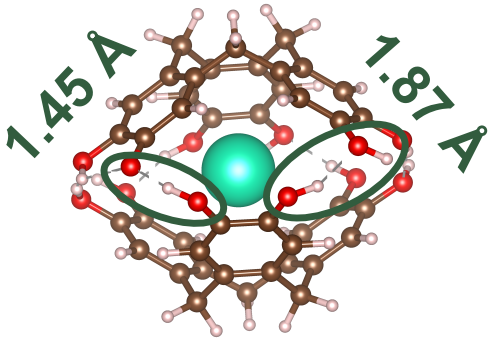

Figure 3: PBEh-3c optimised structure of $[Cs(ctcH_6)(ctcH_5)]$ with $O^-\cdots H-O$ (left) and $H-O\cdots H-O$ (right) hydrogen-bond lengths.

compared to protonation state 12, which is the case for $[Cs(ctcH_6)(ctcH_5)]$, $[Cs(ctcH_5)_2]^-$, $[Cs(ctcH_5)(ctcH_4)]^{2-}$, $[Cs(ctcH_4)_2]^{3-}$ and $[Cs(ctcH_4)(ctcH_3)]^{4-}$. This resulting asymmetry is also reflected by an analysis of the longest and shortest oxygen-oxygen distances between the two CTC units, as shown in Table 1, which shows results for all assessed protonation states. On that note, it is very interesting to observe that a clam-like structure is retained for $[Cs(ctcH)(ctc)]^{10-}$ even though it only contains one single hydrogen bond. We will come back to a similar system with a neutral guest atom later and demonstrate how the positive charge on Cs^+ facilitates the formation of the clam in this case. This shows the importance of the guest in supporting capsule formation.

The $[Cs(ctcH_3)_2]^{5-}$ system (protonation state 6) is held together by six $O^-\cdots H-O$ hydrogen bonds with a $O^-\cdots H-O$ separation of 1.44 Å. Six aromatic rings create a perfect octahedral environment around the Cs^+ atom (see Fig. 4). Further deprotonation i.e. going to $[Cs(ctcH_2)_2]^{7-}$, $[Cs(ctcH_2)(ctcH)]^{8-}$ and $[Cs(ctcH)_2]^{9-}$ introduces $O^-\cdots O^-$ type repulsions to the systems as reflected by increased oxygen-oxygen distances (see Table 1). These clams are no longer "closed" (see Fig. 2c as an example), but in an "opened-up" arrangement. Interestingly, in the $[Cs(ctc)(ctc)]^{11-}$ structure, the clam-shell is completely distorted and consequently Cs^+ does not associate with the aromatic surface of the cyclotricatechylene anions. Rather, it starts interacting with the O^- of one of the phenolic groups (see Fig. 2d). Having established the structural features and most stable protonation states, we continue

our analysis with an investigation of the intermolecular interactions that play an important role in describing the chemical and physical properties of these systems. We first do this qualitatively and then follow with a quantitative study.

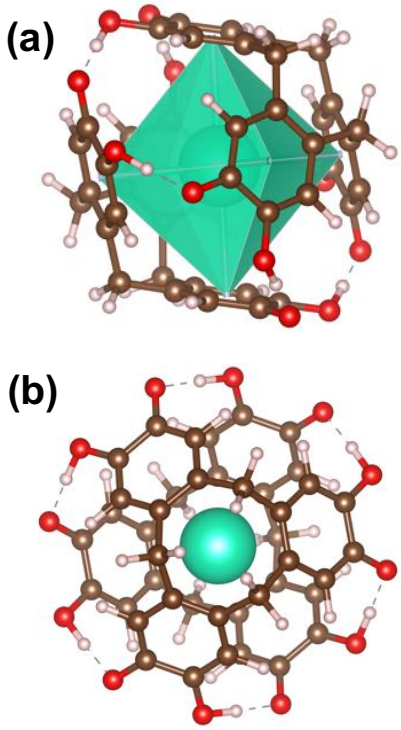

Figure 4: Views of the $[Cs(ctcH_3)_2]^{5-}$ structure (protonation state 6).

3.1.2 Qualitative analysis of noncovalent interactions

In this section, we gain qualitative insights into the CTC-based systems by studying them with the NCIPLOT scheme. This helps us to understand the type of noncovalent interaction that dominates a specific region of the system. NCIPLOT analysis reveals a set of complex interactions that arise in these systems because of hydrogen-bond interactions, van-der-Waals forces, and steric repulsions. As seen in our structural analysis, hydrogen-bond interactions involve the phenolic hydrogens. The internal aromatic surfaces enable van-der-Waals interactions with the enclosed Cs^+. In a single CTC unit, steric strain arises because of its rigid bowl-shaped conformation. In this context, the NCIPLOTs in this manuscript

Table 1: Structural analysis of $(CTC)_2$-Cs^+ systems. The first column represents the protonation state, while the following columns represent the phenolic oxygen-oxygen distances of two interacting CTC units that participate in hydrogen-bond formation or oxygen-oxygen repulsion. Note that we only show the shortest and longest distances. Protonation state 12: closed arrangement with six symmetric $H-O\cdots H-O$ bonds (light green); protonation state 6: closed arrangement (six symmetric $O^-\cdots H-O$ bonds) (dark green); protonation states 11-7: partially opened-up arrangement (light red); protonation states 5-1: completely opened up arrangement (red), and protonation state 0: distorted structure (dark red)

protonation state	shortest O-O distance (Å)	longest O-O distance (Å)
12	2.72	2.73
11	2.48	2.78
10	2.44	2.79
9	2.43	2.79
8	2.42	2.80
7	2.43	2.75
6	2.48	2.48
5	2.46	3.51
4	2.41	3.85
3	2.48	4.01
2	2.45	4.34
1	2.47	4.13
0	4.13	5.11

do not show the purely repulsive interaction region due to clarity reasons, but those are provided in the SI (Figs S3 and S4). Moreover, for the discussion herein, the visualisation of the intermolecular attractive forces is more insightful. For instance, Figs 2b and 5 clearly show how the stability of $[Cs(ctcH_3)_2]^{5-}$ seems to be mainly driven by its $O^-\cdots H-O$ type hydrogen-bonds and larger van-der-Waals interaction regions compared to other protonation states. This is further reason to speculate that that system may be the most stable one; something that will be addressed quantitatively in the following section.

3.1.3 Energetic properties: total intermolecular interaction energies and cooperativity

Having seen a qualitative depiction of the interactions at play, we now proceed with a quantitative analysis. Intermolecular interactions play a very important role in determining the chemical and physical properties in supramolecular chemistry. Therefore, their investigation

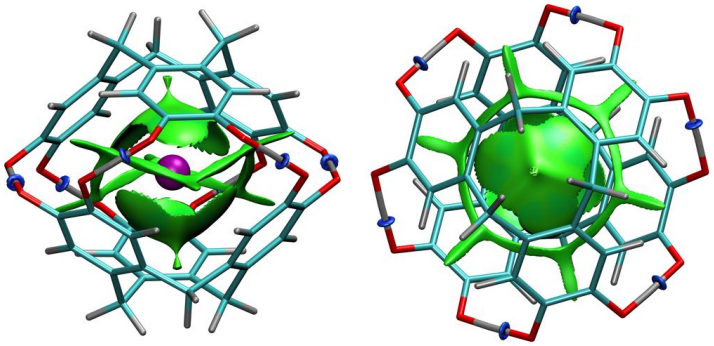

Figure 5: NCIPLOT isosurfaces of the PBEh-3c optimised $[Cs(ctcH_3)_2]^{5-}$ structure. The isosurfaces were generated for a density value of 0.09 a.u. and a reduced density gradient value of 0.3 a.u. The plots show the intermolecular non-covalent interactions between three interacting units. Cs^+-π interaction regions and hydrogen bond interactions are highlighted in the insets. All hydrogens are shown in silver, oxygens in red, carbons in cyan, and caesium in ochre.

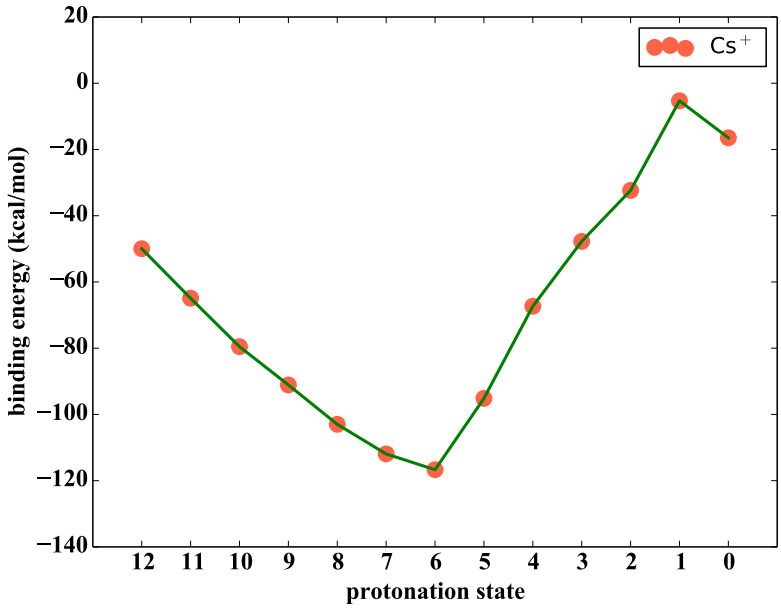

Figure 6: Binding energy analysis of $(CTC)_2$-Cs+ structures (see Eq. 1). Level of theory: ωB97M-V/def2-TZVP+E^{ABC}.

is very insightful. The interaction energy ΔE studied in this work is defined as the difference between the total energy of the trimer and the sum of three monomer energies (see Eq. 1). According to this definition of the binding energy, a negative value indicates the formation of a stable complex.

The binding energy of $[Cs(ctcH_6)_2]^+$ is -49.96 kcal/mol and becomes more negative—i.e. it increases gradually in strength—with the removal of the phenolic protons with $[Cs(ctcH_3)_2]^{5-}$ (protonation state 6) having the strongest net intermolecular interaction with a binding energy of -116.69 kcal/mol (see Fig. 6). This confirms our previously made hypothesis that this protonation state is the most stable, as indicated by its structural features (Section 3.1.1) and NCIPLOTs (Section 3.1.2). Note that about 35.72 % of the total binding energy stem from London dispersion (-41.68 kcal/mol). 3.78% of this dispersion-driven contribution is due to the three-body component from DFT-D3, thus validating our decision to enhance the ωB97M-V method with that term.The binding strength decreases upon further deprotonation (Fig. 6). In fact, when comparing protonation state 6 with states 5 and 7, we observe a decrease of 21.52 kcal/mol in the net interaction strength for the first, and a decrease of 4.76 kcal/mol for the second. The favourable binding energy in protonation state 6, i.e. $[Cs(ctcH_3)_2]^{5-}$, seems most likely to be a result from the high symmetry of the system, which allows the Cs^+ to interact equally with both upper and lower halves, as shown in Fig. 7. The overall stability is further supported by the formation of the shorter hydrogen bonds of the type $O^-\cdots H-O$. An interesting finding is that the $[Cs(ctcH)(ctc)]^{10-}$ structure (protonation state 1) persists the clam shape and Cs^+ interacts with the aromatic π surfaces, while the $[Cs(ctc)_2]^{11-}$ structure (protonation state 0) is fully distorted, with Cs^+ interacting with an O^- group. The latter feature is the reason for the seemingly stronger stability of protonation state 0 compared to protonation state 1, as shown in Fig. 6.

Experimental studies could not provide information on the driving force that is responsible for the stability of these systems. While, unsurprisingly, two-body interactions are the largest contributor to the total binding energies, non-additive (in this case three-body) interactions

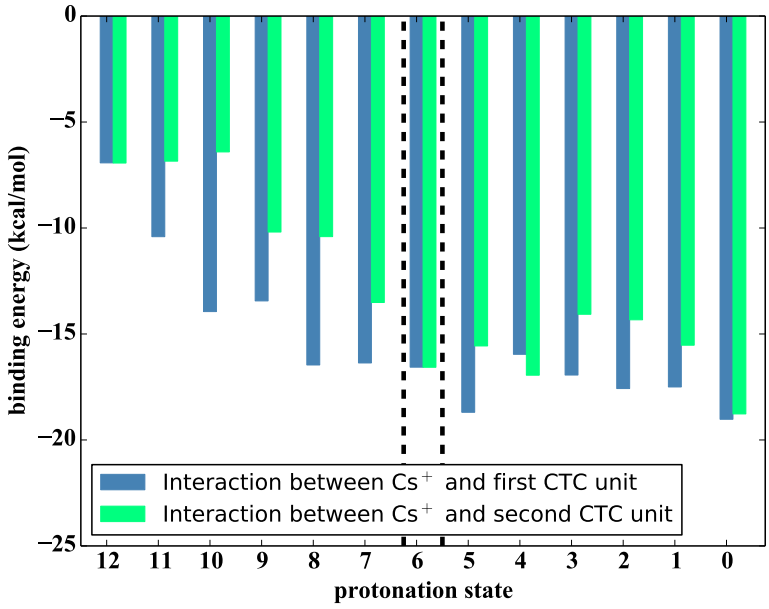

Figure 7: Binding energy analysis of the two CTC units with Cs^+ (see Eq. 3). Level of theory: ωB97M-V/def2-TZVP+E^{ABC}. The area in between the dashed lines highlights the area of maximal overall stability.

cannot be neglected, and in fact determine whether a system is additionally stabilised by cooperative effects or destabilised by anticooperativity. For instance, intermolecular many-body interactions often account for 10-20% of the lattice energy of a molecular crystal,[75,76] while many-body effects in water clusters manifest through cooperative hydrogen bonding, which contributes 30% or more to the total interaction energy.[76,77]

Herein, we investigate the role of cooperative hydrogen bonding and guest-π interactions in the stability of the various CTC-based systems., for which we consider the electronic part (no thermal effects) to examine and eventually understand any potential non-additive effects. Fig. 8 shows the three-body intermolecular interactions of the systems. For a fully protonated structure i.e. $[Cs(ctcH_6)_2]^+$, the three-body intermolecular interaction is nearly additive ($\Delta E_3 = -1.48$ kcal/mol; 2.96 % of the total interaction energy) that means interaction energy of the two CTC units and Cs^+ is merely the sum of dimer interaction energies (compare with Eq. 2). The strength of the three-body intermolecular interaction

increases upon deprotonation of the CTC units (Fig. 8). We see that $[Cs(ctcH_3)_2]^{5-}$ has the maximum stability due to cooperativity (ΔE_3=−12.61 kcal/mol), which contributes 10.80% to the total interaction energy, a significant value.

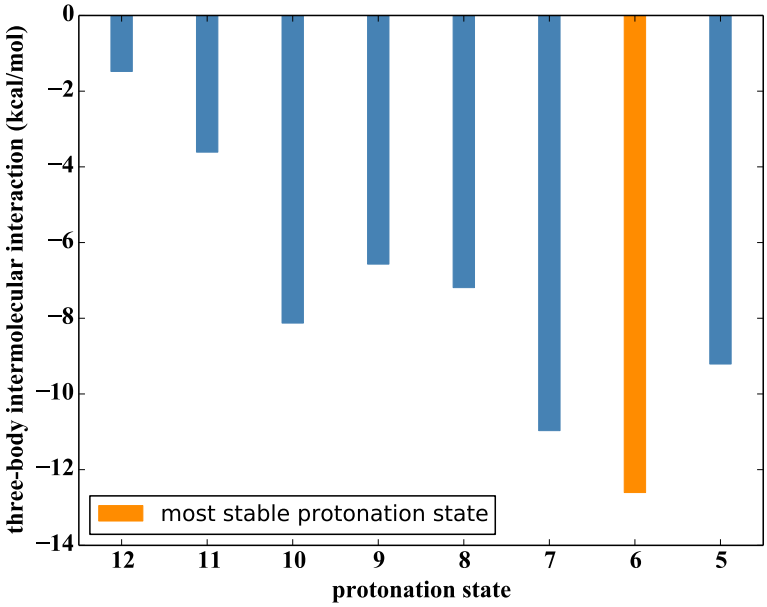

Figure 8: Three-body intermolecular interactions (ΔE_3) of $(CTC)_2$-Cs+ structures (see Eq. 4). Level of theory: ωB97M-V/def2-TZVP+E^{ABC}. ΔE_3<0: cooperative, $\Delta E_3 = 0$: additive and ΔE_3>0: anti-cooperative.

3.2 Group-1 alkali metal cations as guest

CTC-derived clam-like units appear to be promising host systems, particularly for large alkali metal cations, such as Cs^+. In this section, we present the reasonable next step of our analysis, namely the systematic investigation of other group-1 cations to investigate the effect of the size of the guest system before we then continue with an investigation of the effect of the guest's charge in the final two sections of this work.

3.2.1 Structural characteristics

The clam-like assemblies formed by the hydrogen-bonded $ctcH_6$ dimers (protonation state 12) show a tendency for group-1 metal cations. Regardless of the guest, closed capsules are formed with six symmetric H−O···H−O hydrogen bonds that differ, however, in length: 1.78 Å for Cs^+ and Rb^+, 1.80 Å for K^+, 1.84 Å for Na^+, and 1.83 Å for Li^+. After having formed the capsule, the approximate diameter of the equator of a single $ctcH_6$ unit (represented by the longest O-O distance) increases when we move from Cs^+ to Rb^+, K^+, Na^+ and Li^+ (Cs^+: 9.48 Å, Rb^+: 9.54 Å, K^+: 9.62 Å, Na^+: 9.75 Å, and Li^+: 9.72 Å). The twelve aromatic carbons adjacent to the methylene group create the closest contacts with the cation.

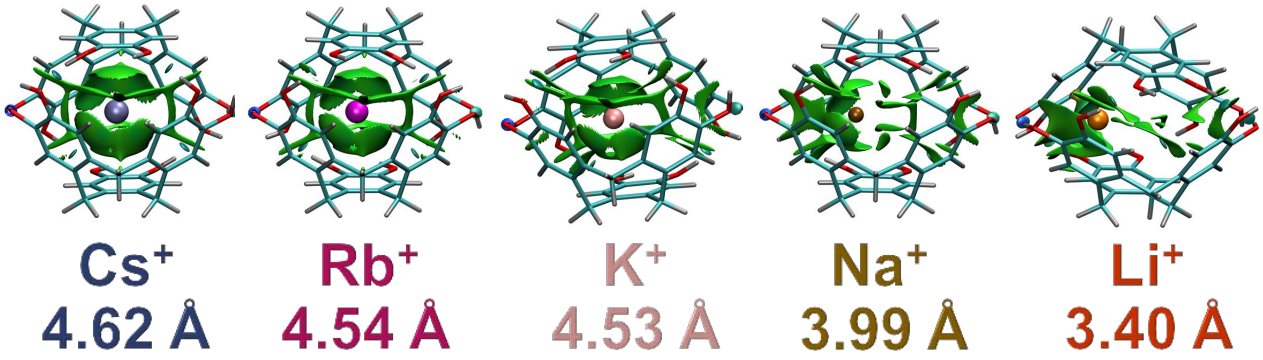

Figure 9: NCIPLOTs of clam-like CTC capsules: alkali metal cation as guest — M^+-O^- distances (protonation state 11)

Next, we explore the structures and stabilities at all other possible protonation states. For $[M(ctcH_6)(ctcH_5)]$ (where M=Cs, Rb, K, Na, and Li), the two CTC units interact through one O^-···H−O bond and five H−O···H−O bonds, as discussed earlier. It is well known that the charge density of the cation increase when we move from the bottom to the top of the first group in the periodic table. Based on our observations, we can conclude that alkali metal cations with higher charge densities prefer to interact with the O^- end of one of the phenolic groups instead of establishing an interaction with the aromatic π surfaces (see Fig. 9).

Because of hydrogen-bond asymmetry in the clam's rim, the $[M(ctcH_6)(ctcH_5)]$, $[M(ctcH_5)_2]^-$,

$[M(ctcH_5)(ctcH_4)]^{2-}$, $[M(ctcH_4)_2]^{3-}$ and $[M(ctcH_4)(ctcH_3)]^{4-}$ structures are slightly "opened-up", where M=Rb, K, Na and Li. For protonation state 6, $[M(ctcH_3)_2]^{5-}$] (where M = Cs, Rb, or K) has a closed and symmetric shape with the largest possible number of $O^-\cdots H-O$ hydrogen bonds ($O^-\cdots H-O$ distance for Cs^+=1.44 Å ; Rb^+=1.44 Å and K^+=1.45 Å). Interestingly, the six $O^-\cdots H-O$ hydrogen bonds are not symmetrically arranged in $[Na(ctcH_3)_2]^{5-}$ and $[Li(ctcH_3)_2]^{5-}$ (see Fig. S6). Moreover, Na^+ and Li^+ are not located at the centre of the clams, but displaced towards one of the oxygens. For the remaining protonation states, the clams are opened up because of the presence of repulsive $O^-\cdots O^-$ interactions.

NCIPLOTs reveal how the type of noncovalent interactions change depending on the different geometrical features of the capsules that contain different guests, and Fig. 9 shows some representative examples. For large alkali metal cations (i.e. Cs^+, Rb^+ and K^+), van-der-Waals interactions are established throughout the cavity. NCIPLOT isosurfaces highlight how Cs^+, Rb^+ and K^+ are held in the centre of the cavity through M^+-π interactions, while Na^+ and Li^+ associate with deprotonated O^- groups (see Fig. 9). The latter can be explained with electrostatic interactions between the positively charge guest and the negatively charged regions of the capsule's shell. In fact, plots of MESPs show the negatively charged regions in Fig. 10 for both $[Cs(ctcH_6)(ctcH_5)]$ and $[Li(ctcH_6)(ctcH_5)]$. While the latter explains the fact that Li^+ is no longer located in the centre of the capsule, there must be a larger force at play that overcomes the attraction to the negatively charged site and keeps Cs^+ in the centre. The most conceivable explanation based on the NCIPLOTs in Fig. 9 are London-dispersion interactions. In fact, Cs^+ has a larger (and softer) electron shell, which is easier to polarise than Li^+. Larger polarisabilities are connected with larger C_6 dispersion coefficients, which are proportional to the dispersion interaction. In fact, an analysis of the system-dependent, atomic C_6 coefficients obtained with the DFT-D3 model—see Refs 45 or 78 for more details of how the coefficients are obtained—confirm our reasoning: the DFT-D3 C_6 for Cs^+ is 649.1 a.u. while it is only 85.3 a.u. for Li^+. This explains why larger guest cations seem to be appropriate guests, as dispersion forces play a crucial role in controlling the geometry of the

host-guest system.

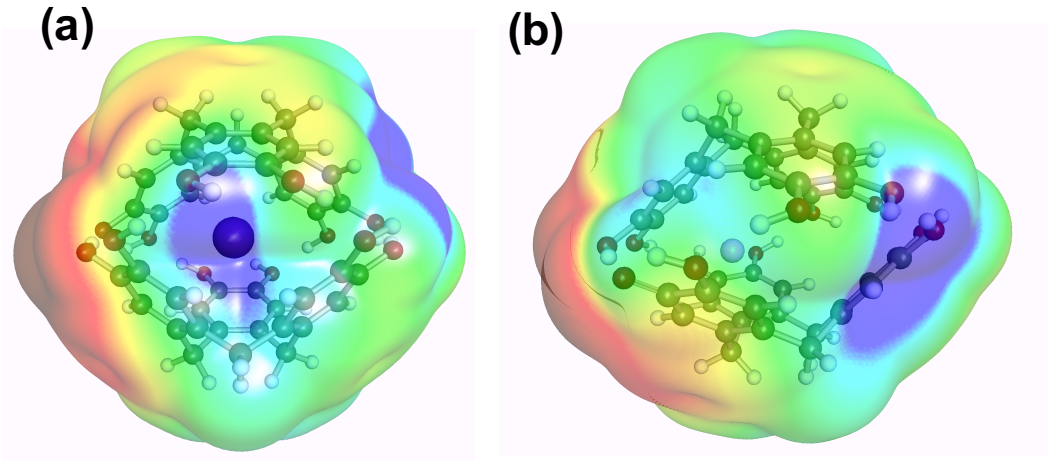

Figure 10: Electrostatic potential functions (EPFs) mapped onto electron density isosurfaces around $[Cs(ctcH_6)(ctcH_5)]$ (a) and $[Li(ctcH_6)(ctcH_5)]$ (b). Positively or negatively charged regions are indicated by color gradients changing from dark blue to red, respectively (PBEh-3c level of theory).

3.2.2 Energetic properties: total intermolecular interaction energies and cooperativity

Our quantitative analysis of the stabilities of the various group-1 based capsules begins with the fully protonated systems. $[Cs(ctcH_6)_2]^+$, $[Rb(ctcH_6)_2]^+$ and $[K(ctcH_6)_2]^+$ have interaction energies of -49.96, -46.51 and -48.86 kcal/mol, respectively. $[Na(ctcH_6)_2]^+$ and $[Li(ctcH_6)_2]^+$ are found to be less stable with binding energies of -31.67 and -15.69 kcal/mol, respectively. In fact, the negative binding energies of the Na^+/LI^+ containing trimers can be explained entirely due to the to CTC halves interacting via hydrogen bonds; the dimer interaction energy between the two CTC units without the presence of Na^+ or Li^+ is about -33.3 kcal/mol in both cases. When we analyse the individual dimer energies between one cation and one of the two CTC units, they are positive, meaning there is no attractive interaction between the two (interaction of Li^+ with either of the two CTC units is $+10.82$ kcal/mol, each; interaction of Na^+ with either of the two CTC units is $+1.88$ and $+1.79$ kcal/mol, respectively).

We now turn towards the estimation of binding strengths for the various deprotonated forms. Unsurprisingly, for all types of guests, the stability increases with deprotonation, which results in systems of the form $[M(ctcH_3)_2]^{5-}$ as being the most stable complexes. The stability of protonation state 6 ($[M(ctcH_3)_2]^{5-}$) is driven by the maximum number of $O^{-}\cdots H-O$ type hydrogen-bond interactions. While these trends reflect our earlier discussion of the Cs^+-based system (see Section 3.1.3), we notice a decrease in stabilities when moving to smaller cations. For instance, there is a decrease of 25.82 kcal/mol in the absolute binding energy when we move from $[Cs(ctcH_3)_2]^{5-}$ to $[Na(ctcH_3)_2]^{5-}$ and a decrease of 35.73 kcal/mol when we move from $[Cs(ctcH_3)_2]^{5-}$ to $[Li(ctcH_3)_2]^{5-}$. We also note that Cs^+, Rb^+ and K^+ interact equally with both the upper and lower CTC units, whereas Na^+ and Li^+ favour interaction with one over the other unit due to the guest no longer being in the centre of the capsule (see Fig. 11). Again, our results can be rationalised by having a look at the DFT-D3 C_6 atomic dispersion coefficients, which decrease with decreasing size of the ions: 649.1 a.u. for Cs^+, 476.3 a.u. for Rb^+, 338.0 a.u. for K^+, 186.1 a.u. for Na^+, and 85.3 a.u. for Li^+.

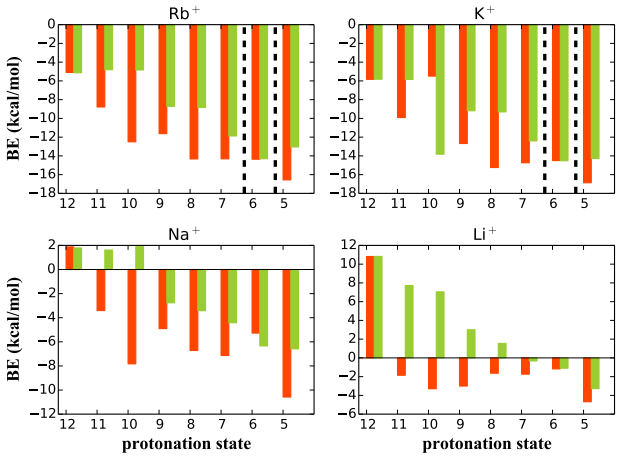

Figure 11: Binding energy (BE) analysis of the two CTC units with M^+ (where M=Rb, K, Na and Li). Level of theory: ωB97M-V/def2-TZVP+E^{ABC}. Interactions between M^+ and the first CTC unit are highlighted in red and between M^+ and the second CTC unit in green.

A comparison of the three-body intermolecular interactions of the various systems reveals large similarities in the results for the capsules that enclose Cs^+, Rb^+ and K^+. For pro-

tonation states 12 ($[M(ctcH_6)_2]^+$) the interaction energies of the two CTC units and the guest cation are nearly equal to the the sum of three dimer interaction energies. The three-body intermolecular interaction terms ΔE_3 becomes more negative upon deprotonation, and protonation states 6 (i.e. $[Cs(ctcH_3)_2]^{5-}$, $[Rb(ctcH_3)_2]^{5-}$ and $[K(ctcH_3)_2]^{5-}$) have the largest stability due to cooperative effects ($\Delta E_3(Cs^+)$=−12.61 kcal/mol; $\Delta E_3(Rb^+)$=−12.37 kcal/mol and $\Delta E_3(K^+)$=−14.06 kcal/mol, respectively). The numbers also indicate a slight increase in the cooperativity when moving to smaller cations, which may again be a result of the higher charge density.

Note that compared to Cs^+, Rb^+, and K^+, we observe a different trend in the three-body interaction for the Na^+ and Li^+ continuing systems. While the total interaction energies have their optimal value for protonation state 6, this is not the case for the value of ΔE_3 where cooperativity increases upon deprotonation beyond protonation state 6 (see Fig. 12). The most likely reason is that for those systems the cations interact with an O^- group in the capsule's shell. The reason why protonation state 6 for these systems is overall the most stable, indicates that its stability is not driven by cooperativity, but by the formation of the CTC dimer via the $O^-\cdots H-O$ type bonds; as discussed earlier, these bonds are the only reason why the capsule forms for these guests.

All our findings on group-1 type guests lead to the conclusion that CTC-based clams have a tendency to accommodate large alkali metal cations through M^+-π interactions that are favoured by larger dispersion interactions. However, we also see that the interplay between dispersion and electrostatics is important and that the latter have an impact on the cooperativity. Our calculations also showed that there could be potential for forming K^+ based capsules subject to finding the right experimental conditions, an endeavour that could be the focus of future experimental studies.

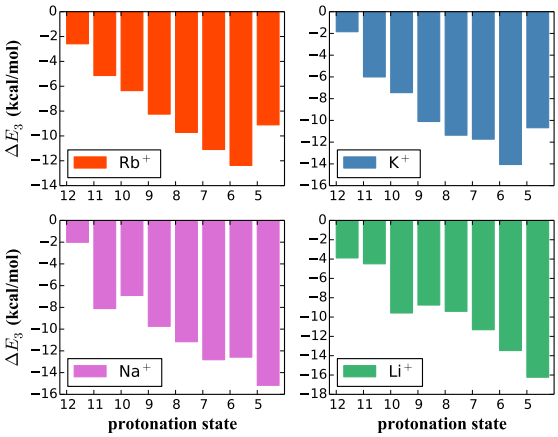

Figure 12: Three-body intermolecular interactions (ΔE_3) of $(CTC)_2$-M^+ structures (where M=Rb, K, Na and Li). Level of theory: ωB97M-V/def2-TZVP+E^{ABC}. ΔE_3 <0: cooperative, $\Delta E_3 = 0$: additive and ΔE_3 >0: anti-cooperative.

3.3 Group-18 noble gas atoms as guest

In the previous section, we have seen that CTC can be a suitable macromolecular unit to selectively detect large group-1 metal cations. We now turn our attention towards the interaction of CTC with noble gas atoms. This study is worthy of investigation as such guests are isoelectronic with group-1 cations, and therefore it is justified to study if they are able to compete with the previously discussed systems.

3.3.1 Structural characteristics

As outlined in the other sections, the two CTC units can interact through two different types of hydrogen bonds. The fully protonated $[Xe(ctcH_6)_2]$ system possesses a clam-like structure with Xe being at the centre. While this is structurally similar to the Cs^+ equivalent, the latter has a more contracted shape with closer contacts between the guest and the aromatic rings: the shortest Cs^+-C distance is 3.51 Å , while the shortest Xe-C distance is 3.65 Å. We see similar observations for the various protonation states (see Table S7). When we analyse the series leading from protonation state 12 to 6, the Xe-based systems have very similar O-O distances between the two halves of the clam compared to the Cs^+-containing

systems. Interestingly, beyond this series, for instance for protonation state 5, these O-O distances are different. For example, the longest $O^{-}\cdots O^{-}$ distance for $[Cs(ctcH_2)(ctcH)]^{8-}$ is 4.01 Å, while it is 5.00 Å for $[Xe(ctcH_2)(ctcH)]^{9-}$ (see Table S8). Most importantly, we also observe the importance of electrostatic interactions between host and guest. For instance, the $[Cs(ctcH)(ctc)]^{10-}$ structure retains the clam-like assembly, but the isoelectronic $[Xe(ctcH)(ctc)]^{11-}$ structure is completely distorted (see Fig. S12), which indicates an importance of having a positively charged guest inside the capsule to maximum electrostatic interactions.

When turning to other noble gas atoms, we note in passing that we observed very similar trends for the isoelectronic pairings Kr/Rb^+ and Ar/K^+ (see Tables S9 and S10). The neon and helium-based systems, however, look structurally different from their respective isoelectronic group-1 counterparts. For instance, unlike Na^+ and Li^+, Ne and He do not interact with the O^- groups (see Fig. S13). Again, the role of the charge seems to be important.

3.3.2 Energetic properties: total intermolecular interaction energies and cooperativity

We now address the interaction energies of the various noble-gas based systems. $[Cs(ctcH_6)_2]^+$ shows the stronger binding strength compared to its $[Xe(ctcH_6)_2]$ cousin ($\Delta E(Cs^+)$=−49.96 kcal/mol and ΔE(Xe)=−42.43 kcal/mol). Interestingly, the difference in the binding energies of Xe and Cs^+ containing capsules increase with deprotonation. In fact, there is a decrease of 44.78 kcal/mol in stability when we move from $[Cs(ctcH_3)_2]^{5-}$ to the isoelectronic $[Xe(ctcH_3)_2]^{6-}$. Note that despite being isoelectronic, Cs^+ has a larger polarisability than Xe (C_6 = 649.1 vs C_6 =290.2, respectively) and therefore is stabilised more by London-dispersion effects. We also note that protonation state 7 is the most stable for the xenon-based capsule, however only by a relatively small margin of 2.6 kcal/mol compared to protonation state 6 (see Table S4), which is why we decided to focus mostly on protonation

state 6 to draw better comparisons with the previously discussed capsules.

When breaking down the total interaction energy into its dimer contributions (see Eq. 2), we note that the CTC-Cs^+ dimer is more stable by 14.22 kcal/mol compare to the CTC-Xe dimer in the case of protonation state 6. We see very similar trends for the isoelectronic Kr/Rb^+, and Ar/K^+ pairs. Smaller noble gas atoms namely He, Ne, and sometimes Ar, show negligible interactions with the two CTC units (Fig. S10) NCIPLOT surfaces highlight how the van-der-Waals-interaction surfaces decrease in size when we move from $(CTC)_2$-Xe to $(CTC)_2$-He system (Fig. S14).

Our analysis of cooperative effects reveals that the presence of a noble gas atom yields a positive value for ΔE_3 for a given protonation state. For instance, the nature of the three-body intermolecular interactions changes from being cooperative to anti-cooperative (ΔE_3=−12.61 kcal/mol for $[Cs(ctcH_3)_2]^{5-}$ to ΔE_3=+9.61 kcal/mol for $[Xe(ctcH_3)_2]^{6-}$).For all other noble-gas containing systems we also find similar anti-cooperative effects for the most relevant protonation states (see Fig. 13).

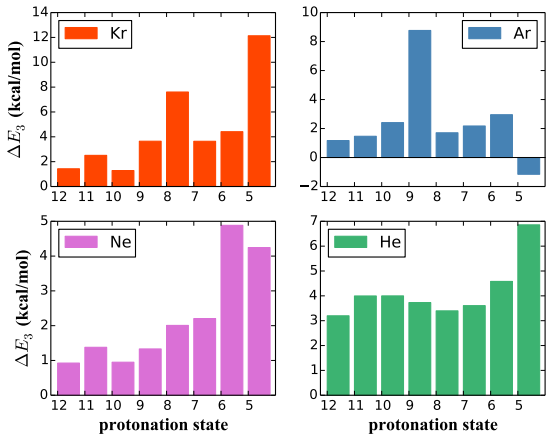

Figure 13: Three-body intermolecular interactions (ΔE_3) of $(CTC)_2$-M structures (where M=Kr, Ar, Ne and He). Level of theory: ωB97M-V/def2-TZVP+E^{ABC}. ΔE_3 <0: cooperative, $\Delta E_3 = 0$: additive and ΔE_3 >0: anti-cooperative.

In summary, in the group-1 based systems the hydrogen bonds and host-guest interactions operate simultaneously to enhance each others' strength, i.e. they act cooperatively. In

the case of noble gas atoms the combined interactions seem to weaken each other and they act anti-cooperatively. The clear difference between the type of guests is the fact that the group-1 based systems contain positively charged guests. Electrostatics therefore seems to play an important role towards the realisation of cooperativity in the most stable systems. Whether this can be enhanced when we increase the charge further, will be seen in the next section.

3.4 Group-2 alkaline earth metal dication as guest

Having established the importance of size and charge of the guest, we conclude our analysis with a brief discussion of group-2 dications. Unlike Cs^+, Rb^+ and K^+, group-2 dications show a tendency to bind with O^- instead of the aromatic π systems. For example, for protonation state 11, the M^{n+}-O^- distance changes from 4.62 Å to 4.38 Å , when we replace Cs^+ with the isoelectronic Ba^{2+} (Fig. 14). Similarly, the M^{n+}-O^- distance changes from 4.54 to 4.12 Å for Rb^+ to Sr^{2+}. We also make very similar observations for K^+ and Ca^{2+}, Na^+ and Mg^{2+}, and Li^+ and Be^{2+}. The consequence of our findings is that CTC derived units distort their shape upon the insertion of group-2 metal dications (see Fig. 15). Given their higher charges, group-2 metal dications have stronger electrostatic interactions compare to alkali metal cations that obviously affect the structural arrangement, but also the interaction

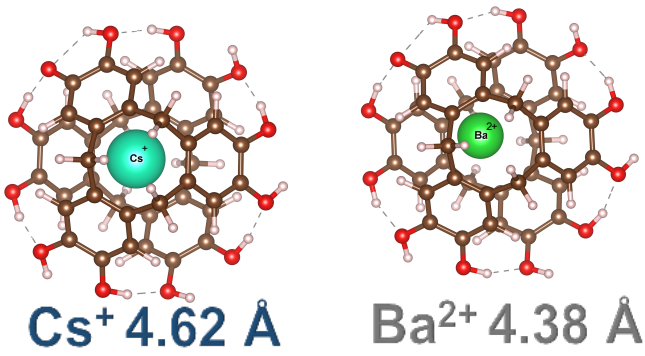

Figure 14: NICPLOTs of clam-like CTC capsules: group-1 and group-2 metal cations as guest—M^+-O^- distances (protonation state-11).

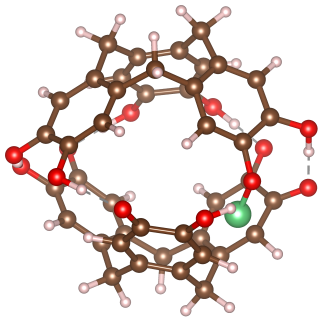

Figure 15: View of the $[Be(ctcH_3)_2]^{6-}$ structure.

energies. For instance, there is an increase of 33.41 kcal/mol in the binding strength when we move from $[Cs(ctcH_3)_2]^{5-}$ to the isoelectronic $[Ba(ctcH_3)_2]^{4-}$. Interaction energies for other protonation stats are listed in Table S11.

Capsules with group-2 metal dications show more negative three-body intermolecular interactions compare to alkali metal cations (ΔE_3=−12.61 kcal/mol for $[Cs(ctcH_3)_2]^{5-}$ to ΔE_3=−22.68 kcal/mol for $[Ba(ctcH_3)_2]^{4-}$). This shows that cooperativity is electrostatically driven and more highly charged guests induce larger cooperativity.

4 Conclusions

Cyclotricatechylene ($ctcH_6$) is a bowl-shaped molecule with six phenolic groups as potential hydrogen-bond donors and acceptors. This hydrogen bond capacity of $ctcH_6$ and its derivatives in various protonation states—collectively referred to as CTC units—can be used to form dimers that resemble the shape of a clam. These supra-molecular assemblies can act as host and accommodate various guests inside it. After initial experimental studies for a few guests and protonation states,[33] open questions remained around the stability of those capsules with respect to different protonation states, as well as size and charge of the guests. To allow treatment of CTC-based clams on an equal footing, we presented a detailed computational study to address those open questions.

Our study began with a detailed screening of more than 4000 structures for a Cs^+ con-

taining CTC_2 capsules that encompassed all thirteen possible protonation states and their isomers. This screening was initially conducted with semi-empirical MO theory and the most stable structures in each protonation state were then further optimised with the low-cost, dispersion-corrected DFT levels B97-3c and PBEh-3c. Intermolecular interactions were interrogated at the ωB97M-V/def2-TZVP+E^{ABC} level, where the suffix indicates that we also took into consideration three-body dispersion effects, something that to our knowledge has not been done before for this particular functional. The quantitative study of intermolecular interactions was additionally guided by qualitative NCIPLOTs and a brief analysis of molecular electrostatic potentials to better understand the role of electrostatic versus London-dispersion interactions. Our comprehensive analysis allowed the following conclusions:

1. The most stable protonation state for all host-guest complexes with cationic guests is protonation state 6, in which six of the phenolic groups were deprotonated and six hydrogen bonds of the type $O^{-}\cdots H-O$ are formed. Protonation state 7 is slightly more stable for capsules with noble-gas atoms as guests.

2. Protonation state 6 also shows the maximal benefits from cooperative three-body effects as long as the guest species is positively charged. Noble gas atoms, which are isoelectronic to the charged species, only showed anticooperative effects. Group-2 cations showed larger cooperative effects than group-1 cations, which indicates that electrostatic effects play an important role in establishing cooperativity.

3. Large group-1 cations sit centrally inside a capsule, while smaller cations tend to move towards the negatively charged sites of the clam shell. We demonstrated how this is due to larger cations having larger atomic dispersion coefficients, which are a result of the larger polarisability of their electron shells. Therefore, dispersion effects play an important role in stabilising the structure. In fact, our findings lead to the conclusion that CTC-based clams have a tendency to accommodate only large alkali

metal cations (i.e. Cs^+, Rb^+ and K^+) through M^+-π interactions that counterbalance any electrostatics effects.

This study has provided useful insights for the design of CTC-based capsules for potential future processes that involve selective recognition and efficient extraction of positively charged species. Based on our findings, we encourage future synthesis of such capsules based on systems containing only six phenolic hydrogens and larger cations. Our work has also revealed how modern computational techniques, particularly recent dispersion-corrected DFT methods, can be used efficiently to gain insights into systems that have previously only been partially interrogated by experiment.

Acknowledgement

This work was supported by an Australian Research Council Discovery Project (DP180101413). N. M. acknowledges a 'Melbourne International Engagement Award (MIEA)' offered through the Melbourne India Postgraduate Program and a 'Melbourne Research Scholarship'. L. G. would also like to acknowledge generous allocations of computational resources from The University of Melbourne and the National Computational Infrastructure Facility within the National Computational Merit Allocation Scheme (project fk5)

Conflict of interest

The authors declare no conflict of interest.

Keywords

Self-assembled capsules; host-guest chemistry; cyclotricatechylene; dispersion-corrected Density Functional Theory, cooperative effects

References

(1) De Greef, T. F.; Smulders, M. M.; Wolffs, M.; Schenning, A. P.; Sijbesma, R. P.; Meijer, E. *Chem. Rev.* **2009**, *109*, 5687–5754.

(2) Cram, D. J.; Tanner, M. E.; Thomas, R. *Angew. Chem., Int. Ed. Engl.* **1991**, *30*, 1024–1027.

(3) Mal, P.; Breiner, B.; Rissanen, K.; Nitschke, J. R. *Science* **2009**, *324*, 1697–1699.

(4) Chakrabarty, R.; Mukherjee, P. S.; Stang, P. J. *Chem. Rev.* **2011**, *111*, 6810–6918.

(5) Kohyama, Y.; Murase, T.; Fujita, M. *Chem. Commun.* **2012**, *48*, 7811–7813.

(6) Yoshizawa, M.; Klosterman, J. K.; Fujita, M. *Angew. Chem., Int. Ed.* **2009**, *48*, 3418–3438.

(7) Kang, J.; Rebek Jr, J. *Nature* **1997**, *385*, 50–52.

(8) Kang, J.; Santamaría, J.; Hilmersson, G.; Rebek, J. *J. Am. Chem. Soc.* **1998**, *120*, 7389–7390.

(9) Cram, D. J.; Cram, J. M. *Container molecules and their guests*; Royal Society of Chemistry, 1997.

(10) Corbellini, F.; Di Costanzo, L.; Crego-Calama, M.; Geremia, S.; Reinhoudt, D. N. *J. Am. Chem. Soc.* **2003**, *125*, 9946–9947.

(11) Kang, J.; Rebek Jr, J. *Nature* **1996**, *382*, 239–241.

(12) Atwood, J. L.; Barbour, L. J.; Jerga, A. *Proc. Natl. Acad. Sci.* **2002**, *99*, 4837–4841.

(13) Ajami, D.; Rebek Jr, J. *J. Org. Chem.* **2009**, *74*, 6584–6591.

(14) Fujita, M.; Tominaga, M.; Hori, A.; Therrien, B. *Acc. Chem. Res.* **2005**, *38*, 369–378.

(15) Kishi, N.; Li, Z.; Yoza, K.; Akita, M.; Yoshizawa, M. *J. Am. Chem. Soc.* **2011**, *133*, 11438–11441.

(16) Stang, P. J. *J. Am. Chem. Soc.* **2012**, *134*, 11829–11830, PMID: 22827533.

(17) Caulder, D. L.; Raymond, K. N. *Acc. Chem. Res.* **1999**, *32*, 975–982.

(18) Jankolovits, J.; Andolina, C. M.; Kampf, J. W.; Raymond, K. N.; Pecoraro, V. L. *Angew. Chem., Int. Ed.* **2011**, *50*, 9660–9664.

(19) Gibb, C. L. D.; Gibb, B. C. *J. Am. Chem. Soc.* **2004**, *126*, 11408–11409, PMID: 15366865.

(20) Conn, M. M.; Rebek, J. *Chem. Rev.* **1997**, *97*, 1647–1668, PMID: 11851461.

(21) Hof, F.; Craig, S. L.; Nuckolls, C.; Rebek, J., Jr. *Angew. Chem., Int. Ed.* **2002**, *41*, 1488–1508.

(22) Hardie, M. J. *Chem. Soc. Rev.* **2010**, *39*, 516–527.

(23) Gutsche, C. D. *Calixarenes: an introduction*; Royal Society of Chemistry, 2008.

(24) Vicens, J.; Harrowfield, J.; Baklouti, L. *Calixarenes in the Nanoworld*; Springer, 2007.

(25) Sliwa, W.; Kozlowski, C. *Calixarenes and resorcinarenes: synthesis, properties and applications*; John Wiley & Sons, 2009.

(26) Steed, J. W.; Zhang, H.; Atwood, J. L. *Supramol. Chem.* **1996**, *7*, 37–45.

(27) Hardie, M. J.; Raston, C. L. *Chem. Commun.* **1999**, 1153–1163.

(28) Holman, K. T.; Atwood, J. L.; Steed, J. W. *Angew. Chem., Int. Ed. Engl.* **1997**, *36*, 1736–1738.

(29) Hardie, M. J.; Ahmad, R.; Sumby, C. J. *New J. Chem.* **2005**, *29*, 1231–1240.

(30) Hardie, M. J.; Mills, R. M.; Sumby, C. J. *Org. Biomol. Chem.* **2004**, *2*, 2958–2964.

(31) Lindsey, A. *J. Chem. Soc.* **1965**, 1685–1692.

(32) Grimme, S.; Brandenburg, J. G.; Bannwarth, C.; Hansen, A. *J. Chem. Phys.* **2015**, *143*, 054107.

(33) Abrahams, B. F.; FitzGerald, N. J.; Hudson, T. A.; Robson, R.; Waters, T. *Angew. Chem., Int. Ed.* **2009**, *48*, 3129–3132.

(34) Holmes, J. L.; Abrahams, B. F.; Ahveninen, A.; Boughton, B. A.; Hudson, T. A.; Robson, R.; Thinagaran, D. *Chem. Commun.* **2018**, *54*, 11877–11880.

(35) Abrahams, B. F.; FitzGerald, N. J.; Robson, R. *Angew. Chem., Int. Ed.* **2010**, *122*, 2958–2961.

(36) Mähler, J.; Persson, I. *Inorg. Chem.* **2011**, *51*, 425–438.

(37) Goerigk, L.; Mehta, N. *Aust. J. Chem.* **2019**, *72*, 563–573.

(38) Bannwarth, C.; Ehlert, S.; Grimme, S. *J. Chem. Theory Comput.* **2019**, *15*, 1652–1671, PMID: 30741547.

(39) Grimme, S.; Bannwarth, C.; Shushkov, P. *J. Chem. Theory Comput.* **2017**, *13*, 1989–2009.

(40) Grimme, S. *J. Chem. Theory Comput.* **2019**, *15*, 2847–2862.

(41) Pracht, P.; Bauer, C. A.; Grimme, S. *J. Comp. Chem.* **2017**, *38*, 2618–2631.

(42) GFN2-xTB V 6.0.1 and above, S.Grimme, University of Bonn, 2018-2019.

(43) J. L. Holmes, B. F. Abrahams, T. A. Hudson, R. Robson, personal communication, publication in preparation.

(44) Brandenburg, J. G.; Bannwarth, C.; Hansen, A.; Grimme, S. *J. Chem. Phys.* **2018**, *148*, 064104.

(45) Grimme, S.; Antony, J.; Ehrlich, S.; Krieg, H. *J. Chem. Phys.* **2010**, *132*, 154104.

(46) Grimme, S.; Ehrlich, S.; Goerigk, L. *J. Comput. Chem.* **2011**, *32*, 1456–1465.

(47) TURBOMOLE V7.3 2018, a development of University of Karlsruhe and Forschungszentrum Karlsruhe GmbH, 1989-2007, TURBOMOLE GmbH, since 2007; available from
`http://www.turbomole.com`.

(48) Ahlrichs, R.; Bär, M.; Häser, M.; Horn, H.; Kölmel, C. *Chem. Phys. Lett.* **1989**, *162*, 165–169.

(49) Eichkorn, K.; Treutler, O.; Öhm, H.; Häser, M.; Ahlrichs, R. *Chem. Phys. Lett* **1995**, *240*, 283–290.

(50) Eichkorn, K.; Weigend, F.; Treutler, O.; Ahlrichs, R. *Theor. Chem. Acc.* **1997**, *97*, 119–124.

(51) Goerigk, L.; Reimers, J. R. *J. Chem. Theory Comput.* **2013**, *9*, 3240–3251.

(52) Goerigk, L.; Collyer, C. A.; Reimers, J. R. *J. Phys. Chem. B* **2014**, *118*, 14612–14626.

(53) Wick, C. R.; Hennemann, M.; Stewart, J. J.; Clark, T. *J. Mol. Model.* **2014**, *20*, 2159.

(54) Klamt, A.; Schüürmann, G. *J. Chem. Soc., Perkin Trans. 2* **1993**, 799–805.

(55) Weigend, F.; Ahlrichs, R. *Phys. Chem. Chem. Phys.* **2005**, *7*, 3297–3305.

(56) Mardirossian, N.; Head-Gordon, M. *J. Chem. Phys.* **2016**, *144*, 214110.

(57) Vydrov, O. A.; Van Voorhis, T. *J. Chem. Phys.* **2010**, *133*, 244103.

(58) Najibi, A.; Goerigk, L. *J. Chem. Theory Comput.* **2018**, *14*, 5725–5738.

(59) Mardirossian, N.; Head-Gordon, M. *J. Chem. Phys.* **2018**, *148*, 241736.

(60) Santra, G.; Sylvetsky, N.; Martin, J. M. L. *J. Phys. Chem. A* **2019**, *123*, 5129–5143, PMID: 31136709.

(61) Mardirossian, N.; Head-Gordon, M. *Mol. Phys.* **2017**, *115*, 2315–2372.

(62) Risthaus, T.; Grimme, S. *J. Chem. Theory Comput.* **2013**, *9*, 1580–1591.

(63) Dobson, J. F. *Int. J. Quantum Chem.* **2014**, *114*, 1157–1161.

(64) Neese, F. *Wiley Interdiscip. Rev.: Comput. Mol. Sci.* **2012**, *2*, 73–78.

(65) DFT-D3 V3.1, S.Grimme, University of Bonn, 2015.

(66) Jurečka, P.; Šponer, J.; Cerny, J.; Hobza, P. *Phys. Chem. Chem. Phys.* **2006**, *8*, 1985–1993.

(67) Řezáč, J.; Riley, K. E.; Hobza, P. *J. Chem. Theory Comput.* **2011**, *7*, 2427–2438.

(68) Goerigk, L.; Hansen, A.; Bauer, C.; Ehrlich, S.; Najibi, A.; Grimme, S. *Phys. Chem. Chem. Phys.* **2017**, *19*, 32184–32215.

(69) Mehta, N.; Casanova-Páez, M.; Goerigk, L. *Phys. Chem. Chem. Phys.* **2018**, *20*, 23175–23194.

(70) Sure, R.; Grimme, S. *J. Chem. Theory Comput.* **2015**, *11*, 3785–3801.

(71) Antony, J.; Brüske, B.; Grimme, S. *Phys. Chem. Chem. Phys.* **2009**, *11*, 8440–8447.

(72) Rezac, J.; Huang, Y.; Hobza, P.; Beran, G. J. *J. Chem. Theory Comput.* **2015**, *11*, 3065–3079.

(73) Johnson, E. R.; Keinan, S.; Mori-Sanchez, P.; Contreras-García, J.; Cohen, A. J.; Yang, W. *J. Am. Chem. Soc.* **2010**, *132*, 6498–6506.

(74) Contreras-García, J.; Johnson, E. R.; Keinan, S.; Chaudret, R.; Piquemal, J.-P.; Beratan, D. N.; Yang, W. *J. Chem. Theory Comput.* **2011**, *7*, 625–632.

(75) Beran, G. J.; Nanda, K. *J. Phys. Chem. Lett.* **2010**, *1*, 3480–3487.

(76) Rezac, J.; Huang, Y.; Hobza, P.; Beran, G. J. *J. Chem. Theory Comput.* **2015**, *11*, 3065–3079.

(77) Kamiya, M.; Hirata, S.; Valiev, M. *J. Chem. Phys.* **2008**, *128*, 074103.

(78) Goerigk, L. In *Non-Covalent Interactions in Quantum Chemistry and Physics*; Otero de la Roza, A., DiLabio, G. A., Eds.; Elsevier: Amsterdam, 2017; pp 195 – 219.

Graphical TOC entry